Simulations and Spectra of Water in CO Matrices

Rafael Escribano*,[1] Emilio Artacho[2], Akira Kouchi[3], Tetusya Hama[3], Yuki Kimura[3], Hiroshi Hidaka[3] and Naoki Watanabe[3]

[1]Instituto de Estructura de la Materia, IEM-CSIC, Serrano 123, 28006 Madrid, Spain

[2]CIC Nanogune and DIPC, Tolosa Hiribidea 76, 20018 San Sebastian; Ikerbasque, Basque Foundation for Science, 48011 Bilbao, Spain; and Theory of Condensed Matter, Cavendish Laboratory, University of Cambridge, J. J. Thomson Ave, Cambridge CB3 0HE, United Kingdom

[3]Institute of Low Temperature Science, Hokkaido University, Sapporo 060-0819, Japan.

*e-mail: rafael.escribano@csic.es

Abstract

Models for the inclusion of water molecules in carbon monoxide matrices are developed using Density Functional Theory applied to amorphous solid systems. The models cover a large range of systems for smaller or larger CO matrices and different water content, consisting in either individual H_2O molecules or small clusters linked by H-bonds. The vibrational spectra of the samples are predicted at the minimum of the potential energy surface. The spectra allow discerning when water molecules remain isolated or forming aggregates, and they also provide an indication of the strength of the H-bonding, when present. The calculations support recent experimental observations that linked IR bands at 3707 cm^{-1} and 3617 cm^{-1} to the presence of unbound water molecules in water-poor CO/H_2O mixed ices. Assignment for some observed bands to water dimers or trimers is offered as well. The residual static pressure in fixed-volume simulation cells is also calculated.

1. Introduction

Ices formed by mixtures of carbon monoxide and water have been studied from different points of view for a long time.[1-3] The small size, physical properties, chemical possibilities and widespread abundance of these molecules have made of the mixed systems a favorite subject for study, both as themselves but also as models for other systems. For instance, the desorption and diffusion of CO in water and in other matrices receive current attention, as shown by a number of papers recently published.[4-10] Also, modifications in the IR spectrum of CO due to the environment are not fully understood.[5,11-15] For example, the presence of water in the sample seems to induce a splitting of the strong IR band at 2138 cm^{-1} characteristic of pure CO. Moreover, the active role of CO and H_2O in astrochemistry, in the gas phase and in heterogeneous reactions involving ice, is also particularly interesting.[16-19] From a

theoretical point of view, several investigations by means of molecular dynamics or ab initio calculations have also enlarged the literature on these systems.[5,20,21]

A novel method for the generation of high-density amorphous ice by a matrix sublimation technique has just been reported.[22] In that paper, a CO: H_2O mixture with high CO concentration was deposited at low temperature (8-10 K) and ultra-high vacuum. The CO matrix containing sparse water molecules was warmed until CO sublimation at 35 K, leaving an amorphous ice residue with special characteristics of large porosity and yet high intrinsic density. The evolution of the CO/ H_2O mixtures was followed by ultra-high vacuum (UHV) transmission electron microscopy (TEM) and Fourier Transform Infrared (FTIR) spectroscopy. The method can be applied to other matrices, like those formed using Ar or N2, but the CO/ H_2O mixture is particularly important for several reasons, outlined above.

In this investigation we follow the work of Kouchi *et al*.,[22] where H_2O molecules at low concentration were inserted in a CO matrix, and we focus on the spectra of water under such conditions, and more particularly, on the high-frequency region around 3000 - 3700 cm^{-1}. We make theoretical models for CO/ H_2O mixtures, and predict their spectra, aiming to analyze and explain the experimental features observed in Kouchi *et al*.[22] The use of these models allows also investigating static stress effects in the mixtures, resulting from the introduction of water molecules within a CO framework.

2. Theoretical models

The ice mixtures studied in ref. Kouchi *et al*.[22] contained CO: H_2O ratios of 10:1 and 50:1. Our aim in this work was to build models for H_2O molecules within rich CO environments but yet to keep the number of molecules within limits that allowed for a large number of calculations. Thus, we chose two basic systems, with 16 and with 32 CO molecules, and in each case we replaced various CO molecules by H_2O molecules, to generate small-matrix or large-matrix samples. At the deposition conditions of low pressure (1 x 10-6 Pa) and temperature (8 K) of Ref. 22, pure CO crystallizes in a primitive cubic lattice of the $P2_13$ space group,[23,24] with a = 5.63 Å and 4 CO molecules per unit cell. We therefore formed our initial CO structures by putting together four (2x2x1) and eight (2x2x2) unit cells yielding supercells of 16 and 32 CO molecules respectively. For the mixtures, we built a number of samples by replacing from one up to 4 (7 molecules in one case, commented on below) CO molecules from the cell by H_2O molecules. Replacement criteria were various: proximity between water molecules, in order to favor the formation of H bonds; or the other way around, remoteness, within the limitations of the cell, to keep the water molecules away from each other; or direct insertion of trimer or tetramer water clusters. For completeness of the study, we induced an amorphous state on some of the samples by means of a Monte Carlo method described below. In this way we generated a large number of samples, so that we could take some statistical conclusions which are presented in the Results section.

The initial structures thus formed were then refined searching for the minimum in their Potential Energy Surface (PES). At that point the atomic force constants and charge distribution were calculated, and the harmonic vibrational spectrum was predicted. Most calculations were carried out using CASTEP,[25] a module of the Materials Studio[26] package that uses plane waves as basis functions and norm-conserving pseudopotentials[27] to describe the effect of core electrons. All calculations were done using Density

Functional Theory (DFT), within the generalized gradient approximation (GGA) as defined in the Perdew-Burke-Ernzerhof (PBE) functionals.[28] We tested several functionals and chose PBE because it yielded vibrational frequencies in better agreement with experiments. Convergence limits for the geometry relaxation were 5.0 x 10^{-6} eV/atom for the energy, 0.01 eV/ Å for the forces, 0.02 GPa for the internal stress and 5.0 x 10^{-4} Å for the displacements. When saddle points instead of global minima in the PES were found, revealed by the presence of imaginary frequency values in the vibrational normal modes, further relaxation was sought using SIESTA.[29-31] The SIESTA method uses Numerical Atomic Orbitals (NAO) as basis sets and norm-conserving pseudopotentials for the core electrons of each atom.[32,33] Again we ran several tests for all parameters involved in the calculations, and selected 0.0001 eV/ Å for the force tolerance, 0.005 Å for the displacements, 0.1 GPa for the stress and a mess cutoff of 300 Ry, which had to be increased to 500 Ry in some cases to avoid the egg-box effect.[30]

The generation of amorphous structures was done using the Amorphous Cell module of Materials Studio.[26] This program creates three-dimensional periodic structures of molecular systems, where the amorphous character is achieved by neglecting any long-range order and minimizing short-range atomic interactions by the Monte Carlo method. A chosen number of molecules are placed inside a cell for a given density and temperature to define the system. For our purposes, we started from some of the crystalline frames mentioned above, which lost their crystalline structure during the amorphous-conversion process. The resulting samples were subsequently optimized and processed in a similar way to that indicated above for the crystalline samples. An example of this process is shown in Fig. 1, bottom panel.

3. Results

Taking into account the number of systems that we have studied, we had to devise a nomenclature to label them. The adopted code started with the number of CO molecules in the system after replacement by H_2O molecules. For instance, *14CO-* indicates that 14 CO molecules remain from a small-matrix sample of 16 CO molecules. Then, the number of inserted water molecules is given, with a capital W, and a letter to distinguish among cases with the same molecular content. Thus, the root *14CO-2W* stands for all cases where, from a small-matrix sample with 16 CO molecules, 14 CO molecules remain and 2 H_2O molecules have been inserted. A suffix *a, b, c…* distinguishes samples with the same CO and H_2O content, but with different molecular structure. When the inserted water molecules formed a cluster, the structure is labeled with an indication of the type of cluster, usually trimer or tetramer (*-triW* or *-tetraW*, respectively), in a nearly linear or angular configuration (*-lin* or *-ang*, respectively). Therefore, *29CO-triW-lin* designates a sample where a water trimer with an approximate linear configuration has been inserted, replacing 3 CO molecules from a large-matrix with 32 CO molecules. For amorphous samples the suffix *amorp-* is added. Fig. 1 represents six of these structures for illustration.

The full list of systems studied in this work is assembled in Table S1 in the Supplementary Material. In this section we concentrate on the most representative cases, listed in Table 1. Our results are presented in subsections dealing with specific aspects: types of binding of water molecules within the sample, predicted spectra, and pressure effects.

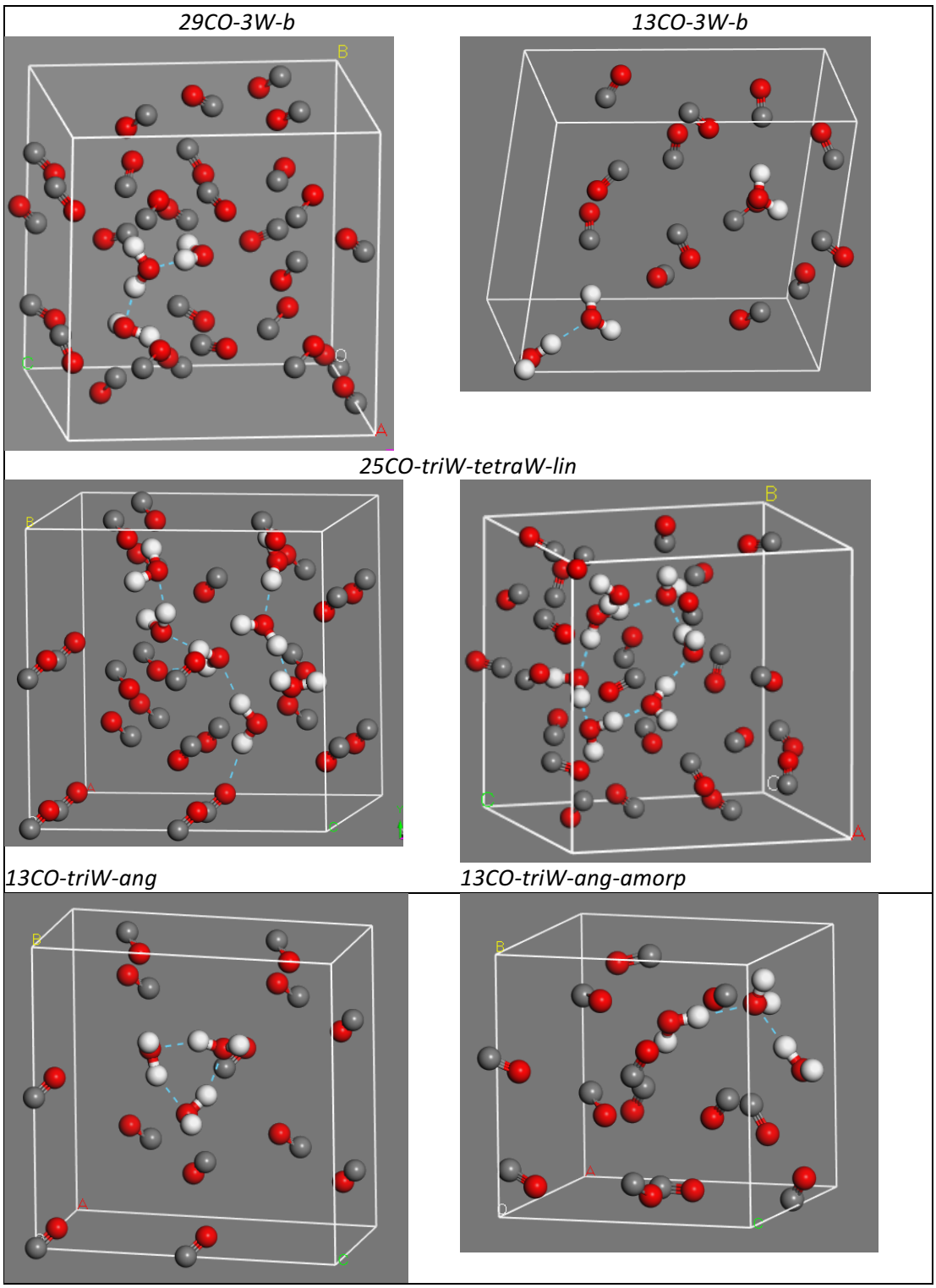

Fig. 1. Examples of structures calculated in this work. Top: *29CO-3W-b* and *13CO-3W-b*; middle: *25CO-triW-tetraW-ang* before (left) and after (right) the relaxation process; bottom: left, *13CO-triW-ang,* initial crystalline structure with water trimer inserted; right, *13CO-triW-ang-amorp,* structure after the amorphous-conversion process. H-bonds are shown by blue broken lines. Capital letters O, A, B and C indicate the origin and the crystalline axes. They are rotated to achieve the clearest display.

3.1 Water binding

From the initial structure of the samples to their final configuration several processes took place. Atomic and molecular rotations and displacements during the search for the minimum of the PES usually involved the creation or breakdown of H-bonds. The presence or absence of H-bonds is indicated in Table 1 for several cases of each type of configuration. A H-bond was acknowledged when the H…O separation was ≤ 2.2 Å and the bonding angle was ≥ 120 ^{o}. H-bond distances are listed in the Table. We have represented unbound water molecules by *mon* and H-bound water molecules by W…W. The results in Table 1 indicate that in large-matrix samples, there are practically no important variations from the initial to the final structures, but in small-matrix samples H-bonds are often created or reinforced with shorter H…O distances when they existed originally.

The initial structure of clusters was optimized separately, apart from the CO network. We generated two trimers, one with a quasi linear structure and the other with a triangular shape, and two tetramers, one again quasi linear, and the other one forming a nearly planar square. For easy reference, they are labelled *triW-lin, triW-ang, tetraW-lin* and *tetraW-ang*, respectively. They are shown in Fig. S1 of the Supplementary Material. Once converged, each cluster was inserted in the CO net after creating an empty space by removal of the appropriate number of CO molecules, and then the usual relaxation process began. H-bond distances quoted in the table for the initial stage of these samples correspond therefore to the geometry of the clusters calculated as isolated species. We can see that the existing H-bonds were strengthened during the refinement of the sample structure. It is interesting also to look at the amorphous case listed in the Table. After inclusion of an optimized water trimer in the CO crystal, an amorphous sample was generated by the process indicated above, which broke all three H-bonds initially present. However, during optimization of the geometry, two H-bonds were created again.

Table 1. Initial and final structures of the water molecules present in selected samples. *mon* is used to represent unbound water molecules and W…W to indicate water molecules linked by a H-bond. For these cases, the H…O distance of the H-bond is quoted in Å.

	Initial	Final
	Structure (H-bond distance/Å)	Structure (H-bond distance/Å)
large-matrix (from 32 CO matrix)		
30CO-2W-b	mon,mon	mon,mon
30CO-2W-c	W…W (1.9)	W…W (1.9)
29CO-3W-b	W…W…W (1.9,1.9)	W…W…W (1.9,1.9)
28CO-4W	mon,mon,W…W (2.0)	mon,W…W…W (2.1,2.1)
small-matrix (from 16 CO matrix)		
14CO-2W-b	mon,mon	W…W (1.9)
13CO-3W-d	mon,W…W (2.2)	W…W…W (1.9,1.9)
12CO-4W-a	mon,mon,mon,mon	mon,W…W…W (1.8,1.9)
12CO-4W-d	W…W,W…W (2.0,2.0)	W…W…W…W (1.9,1.9,2.0)

H2O clusters		
29CO-triW-lin[a]	W…W…W (1.8,1.9)	W…W…W (1.8,1.8)
28CO-tetraW-lin[a]	W…W…W…W (1.9,2.0,2.0)	W…W…W…W (1.8,1.8,1.9)
25CO-triW-tetraW-lin	W…W…W;W…W…W…W (1.8,1.9;1.9,1.9,2.0)	W…W…W…W…W…W…W (1.7,1.8,1.8,1.8,1.8,2.0)[b]
13CO-triW-lin[a]	W…W…W (1.8,1.9)	W…W…W (1.7,1.7)[c]
12CO-tetraW-lin[a]	W…W…W…W (1.9,2.0,2.0)	W…W…W…W (1.8,1.8,1.9)
Amorphous		
13CO-triW-ang-amorp[a]	mon,mon,mon	W…W…W (1.9,2.0)

[a]Initial structure of clusters calculated for the isolated species

[b]Closed ring structure

[c]Very strong H-bonds

Changes in the structures during the geometry optimization process could be followed using the available visualization techniques. Thus, we noticed that the general trend was for O atoms not to move significantly from their initial positions, whereas the H atoms did reorient themselves looking for stronger binding with neighboring molecules.

3.2 Calculated spectra and comparison to observed spectra

Once a good relaxation of the structure was achieved, which placed the systems at the minimum of their PES, the harmonic vibrational spectrum was predicted. We focused on the part of the spectrum corresponding to the O-H stretching vibrations, which can reach between 2500 and 3800 cm^{-1}. Whereas the intramolecular O-H modes fall in the higher wavenumber portion of this range, in the lowest wavenumber region the O…H modes of H-bound structures appear normally. Characteristically, H-bonds are longer and weaker than intramolecular O-H bonds, and consequently they are red-shifted from the other O-H bonds in the spectrum. They are strong, wide features, because they involve large dipole moment variations and a variety of geometrical configurations.[34] The red-shift and strength of these modes is satisfied in the spectra calculated for the samples studied here. Unfortunately, the theoretical model does not provide any information on the width of the spectral modes, and that typical characteristic of H-bond vibrations is missing from the calculations.

Some of the structures contained unbound water molecules (monomers), with or without the presence of other water molecules linked by H-bonds. Whenever there was a monomer, its two stretching modes were predicted at ~ 3750 cm^{-1} (asymmetric stretch, strong) and ~3650 cm^{-1} (symmetric stretch, medium). The upper panels of Fig. 2 display spectra of two samples, one with 2 isolated monomers (left), and the other one with one monomer plus a water dimer. Besides the monomer modes, those of the dimer appeared for the second species at 3721 cm^{-1}, 3717 cm^{-1} (asymmetric stretching), 3629 and 3515 cm^{-1}, the last one being the typical stretching mode of the O…H-O binding, very strong and red-shifted with

respect to the other stretching vibrations. The spectra represented in the lower panels of Fig. 2 are those of samples where no unbound H_2O molecules were present. The corresponding O-H stretching modes at ~ 3750 cm^{-1} and ~3650 cm^{-1} are missing. The spectrum on the left corresponds to the *13CO-triW-lin* structure, created by insertion of a quasi-linear water trimer into the CO net, which developed the strongest H-bonds of all systems, with O…H distances of only 1.7 Å. The H-bond mode was very strong and appeared as low as 3084 cm^{-1}. Finally, the spectrum on the right is that of the amorphous structure listed at the end of Table 1. Two H-bonds linked the three water molecules in a triangular shape.

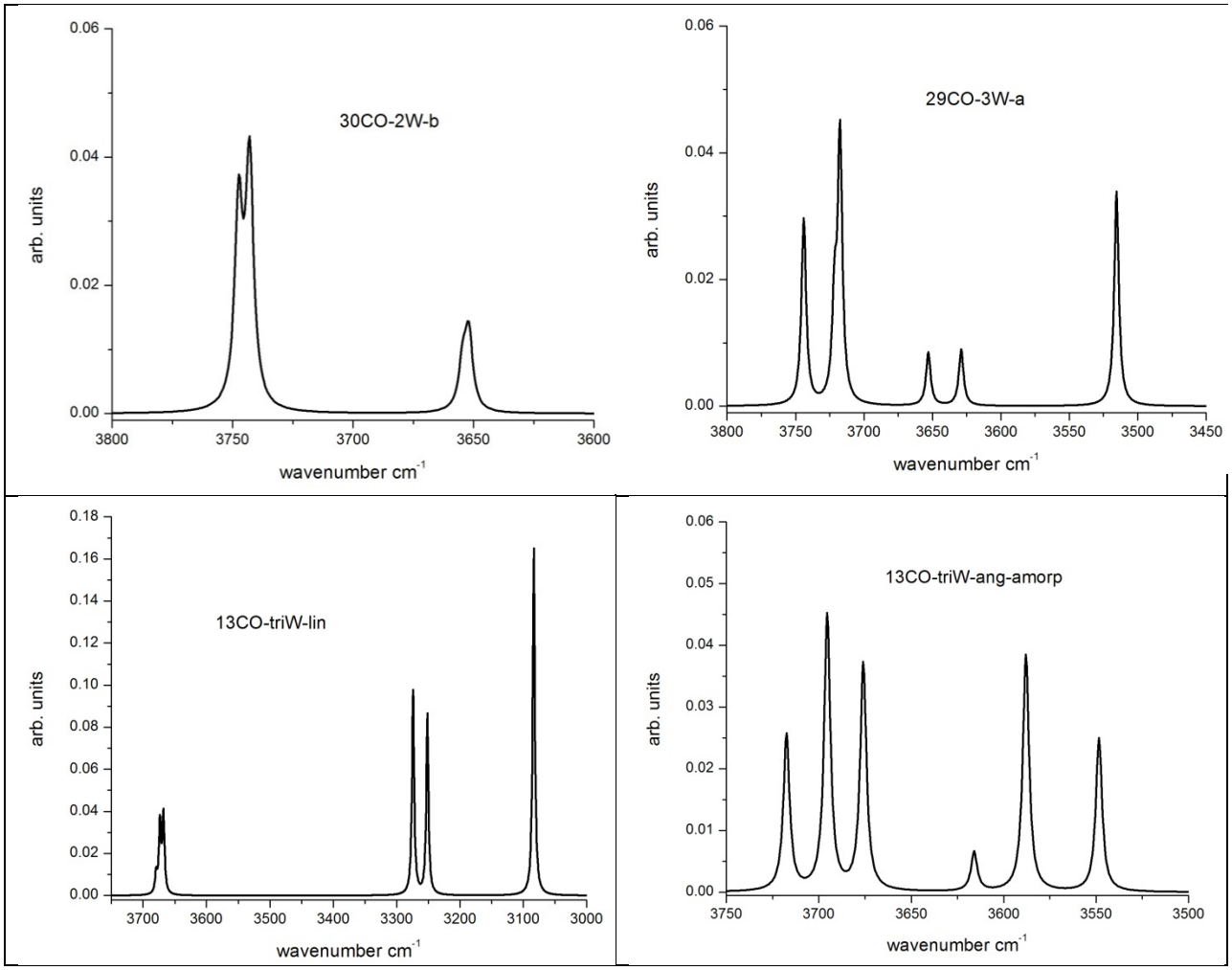

Fig. 2. Upper panels: Spectra from two large-matrix samples. Left: *30CO-2W-b;* both H_2O molecules are unbound; right: *29CO-3W-a*; one of the H_2O molecules is unbound; the other two are linked by a H-bond. Lower panels: Spectra of small-matrix samples, where all H_2O molecules are linked by H-bonds. Left: *13CO-triW-lin*, the species with strongest H-bonds; right: *13CO-triW-ang-amorp*, amorphous sample where the H_2O molecules adopt a near-ring triangular structure. Abscissa scales differ for each spectrum.

The predicted spectra could be compared to the observations of Kouchi *et al*.[22] Before attempting such comparison, though, it was necessary to correct the calculated spectra by the effects of anharmonicity, which was not taken into account in our harmonic calculations. For O-H stretching modes, this is normally done by applying a 1 % reduction on the calculated wavenumbers. We reproduce in Fig. 3 the observed spectra of the water-poor (above) and water-rich CO: H_2O mixtures deposited at 10 K from Kouchi *et al*.[22] The most remarkable feature when looking at these two spectra was the presence of the bands associated to the O-H modes for the monomer in the water-poor sample, at 3707 and 3617 cm^{-1}, which were missing in the water-rich sample. This effect is highlighted by broken lines in both spectra. All other features could be seen in both spectra, although with different intensity and, in some case, different width as well. We present in Table 2 a summary of the stronger IR bands in the observed spectra of Kouchi *et al*.,[22] together with anharmonicity corrected calculated values, for the samples shown in Fig. 2. Based on the structure of these theoretical samples, we put forward in Table 2 a tentative assignment for the experimental peaks. It must be born in mind that the calculated values listed in Table 2 correspond to the species indicated which are taken as representatives, and actual values for other samples may differ within reasonable limits. In all cases where unbound H_2O molecules are present, the corresponding O-H stretching modes appear very close to the 3750 cm^{-1} and 3650 cm^{-1} mentioned above.

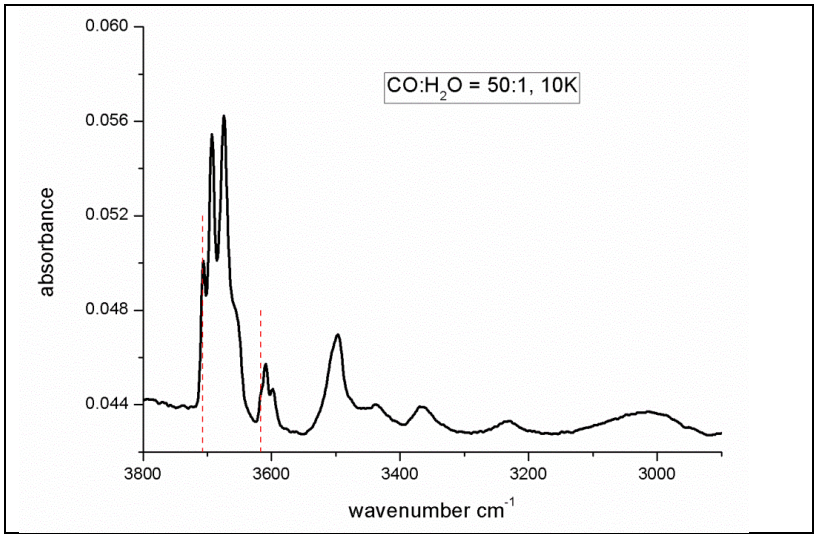

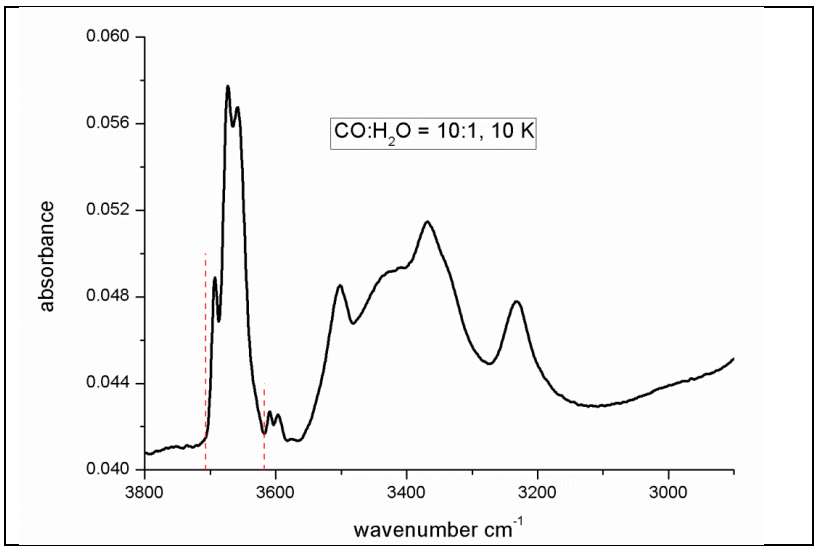

Fig. 3. Observed spectra of water-poor (above) and water-rich samples deposited at 10 K.[22] The dotted lines indicate where the modes of the unbound H_2O monomers appear in the large-matrix samples and are missing in the other case.

Table 2. Tentative assignment for the main peaks observed in the spectra of Fig. 3, adapted from Kouchi *et al*.[22] The assignments are based on the calculated spectra of the samples in Fig. 2, which contained unbound H_2O molecules (monomers) and H-bond structures with 2 or 3 H_2O molecules (W…W and W…W…W, respectively). All values in cm^{-1}.

Mode	Observed	Calculated (anharmonicity corrected)			
		large-matrix		small-matrix	
		Monomer	W…W	W…W…W	W…W…W
ν_3 asym	3707*	3710,3706			
ν_3 asym	3692		3683	3642	3680
ν_3 asym	3674		3680	3637	3658
ν_3 asym	3658			3631	3639
ν_1 sym	3617*	3618,3615			
ν_1 sym	3610		3592		
ν_1 sym	3598				3580
ν H-bond	3495		3480		3552,3512
ν H-bond	3364				
ν H-bond	3232			3241,3218	

*Observed only in water-poor spectra.

3.3 Pressure evolution

The matrix sublimation method described in Kouchi *et al*.[22] generated a high-density amorphous ice. Analysis of UHV-TEM results indicated that, after evaporation of all CO molecules, the resulting ice structure corresponded to that of a 0.1 GPa sample, with an average d-space of 3.1 Å. In an attempt to simulate this experiment, we have carried out a calculation on an already converged structure, *13CO-triW-lin*. The sample was generated with a density of 0.972 g cm^{-3}, yielding a static pressure of 7.6 kBar (0.76 GPa) after the relaxation of the molecular structure. This pressure corresponds to the use of a fixed-size cell, taken from the crystalline structure of CO, which would be different to a theoretical value predicted at zero pressure. The actual value of 0.76 GPa is ruled by the approximations and parameters involved in the calculation, like base error, choice of pseudopotential functions, etc., and should not be compared to any experimental measurement. To check the effects of external pressure on the optimization process, we performed a series of calculations using the Target Pressure option of the Siesta method. First we set a higher external target pressure of 1.0 GPa and unconfined the size of the cell to accommodate to that pressure. A good convergence was achieved, with volume shrinkage from 713 $Å^3$ to 674 $Å^3$, and an energy increase from -9151.18 eV to -9150.99 eV. In another calculation the cell size was released and the pressure was unconstrained. In this case, the volume expanded up to 890 $Å^3$ and the energy dropped to -9151.5174 eV, with null static pressure left. These results show that a good convergence can be achieved for a sample under pressure, where the final configuration shrinks with increasing pressure and the relaxation energy increases. We carried out similar calculations on several other samples, with the results collected in Table 3. While the absolute pressure values are not to be compared to the experimental ones, the results indicated that a theoretical study on the pressure effects could in principle be undertaken using the available tools.

Table 3. Changes upon cell size release. Units are: volume, $Å^3$; pressure, kBar; energy, eV.

		Initial values	Final values
large-matrix (from 32 CO matrix)			
29CO-3W-0	Volume	1427	1765
	Pressure	7.80	0.00031
	Energy	-18669.32	-18669.98
small-matrix (from 16 CO matrix)			
13CO-3W-d	Volume	702	864
	Pressure	7.39	0.00013
	Energy	-9150.730	-9451.038
13CO-3W-c	Volume	738	875
	Pressure	4.85	0.00020
	Energy	-9150.994	-9151.260
12CO-4W-b	Volume	713	858
	Pressure	5.61	0.00022
	Energy	-9028.473	-9028.709
H_2O clusters			
29CO-triW-lin	Volume	1427	1764
	Pressure	8.15	0.00002
	Energy	-18669.39	-18670.11

13CO-triW-lin	Volume	714	890
	Pressure	7.58	0.0014
	Energy	-9151.176	-9151.517
	Volume		674
	Pressure		10.00 (Target pressure)
	Energy		-9150.989
Amorphous			
13CO-triW-ang-amorp	Volume	714	861
	Pressure	6.04	0.0006
	Energy	-9151.020	-9151.25
13CO-triW-lin-amorp	Volume	714	867
	Pressure / kBar	6.08	0.0006
	Energy / eV	-9150.887	-9151.168

Both in the fixed-cell and in the compressed structures of *13CO-triW-lin*, the water molecules were linked by H-bonds of 1.8 Å length forming chains, but the chain was bent in the fixed cell and almost linear in the 1.0 GPa case. The corresponding structures are schematically depicted in Fig. 4. These different structures were also reflected in the radial distribution function (RDF) for the O-O distances for these two samples. We show in Figure 5 the RDF of the samples. The first peak in the RDF graphs corresponds to the O-O distance between H_2O molecules linked by H-bonds, and successive peaks correspond to O-O distances among CO molecules. Values above 5 Å refer to distances between molecules in neighboring cells. Under pressure, the distances among CO molecules shortened a little, whereas those among the H-bonded H_2O molecules were slightly enlarged as a consequence of the linear structure that the W…W…W molecules adopted in this sample.

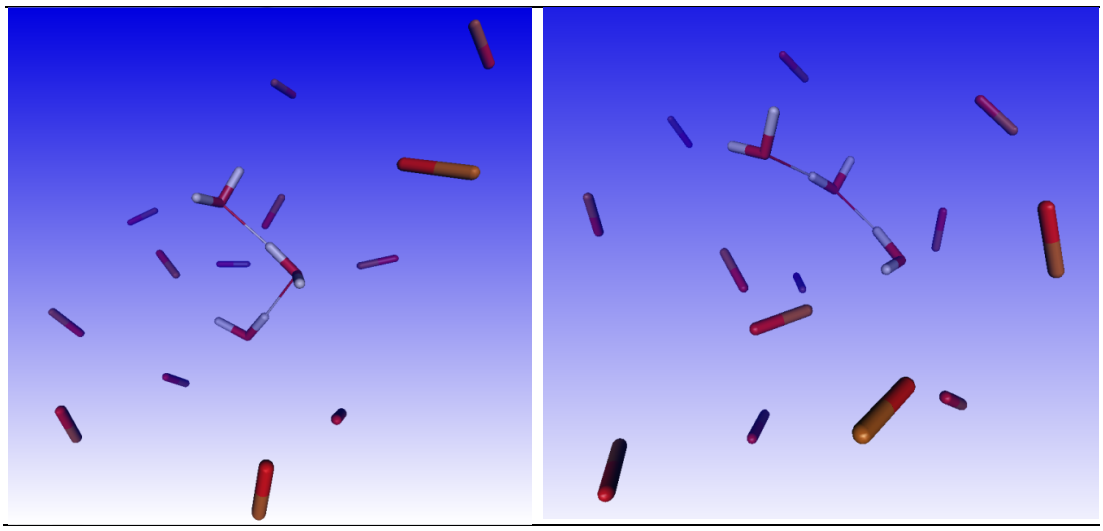

Fig. 4. Schematic representation of the *13CO-triW-lin* structure after geometry relaxation. Left: fixed-cell structure (0.76 GPa), where the water trimer W…W…W had a bent shape; right: relaxation at slightly higher pressure (1.0 GPa); the water molecules took an almost linear configuration.

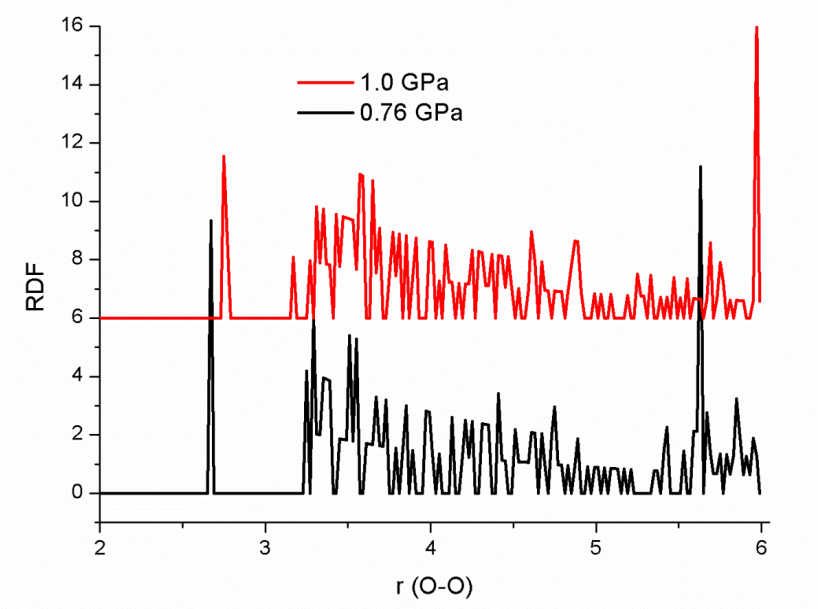

Fig. 5. Radial distribution function (RDF) of O-O distances (in Å) in *13CO-triW-lin*, for the fixed-cell structure (below) at 0.76 GPa and for the higher pressure case (above), at 1 GPa. Higher pressure graph offset in vertical axis for clarity.

4. Summary and conclusions

This paper presents theoretical calculations on models for the inclusion of water molecules into a CO matrix. Many systems are studied with different water contents and distribution, for two basic models denoted large-matrix and small-matrix. The models are built by replacing CO molecules from CO crystalline supercells by H_2O molecules, followed by relaxation of the structure and calculation of the vibrational spectrum. The relaxation process allows following changes in the binding among the water molecules present, including the formation or breakdown of H-bonds. Residual pressure effects in the sample cell are studied in relation to the size of the cell. The main conclusions of this work are listed below.

The methodology employed in this work allowed studying many systems at a reasonable theoretical level, covering many possible configurations of water molecules inside a CO matrix. The water molecules were inserted isolated from each other or linked among themselves by H-bonds as dimers, trimers or higher order clusters. The general trend for water molecules was, for large-matrix systems to remain in their initial configuration, either unbound or forming small clusters, and for small-matrix cases, to build

up new or stronger H-bonds. Similar results were obtained for structures which were made amorphous before the relaxation process.

The calculated vibrational spectra in the O-H stretching region were a powerful tool to reveal the structure of the sample. Some features were very specific in the spectra. First, the presence or absence of the highest frequency peak in this region, near 3750 cm^{-1}, was a firm key to indicate the presence or absence of water unbound molecules. This was assigned to the strong asymmetric O-H stretching mode, and was accompanied by the symmetric stretch, at 3650 cm^{-1}, although this mode is weaker and may be harder to detect.

The corresponding asymmetric and symmetric stretching modes in the spectra of structures with bound water molecules appeared at slightly lower frequencies, usually in decreasing wavenumber order for longer water clusters, but this was not always the case, as some clusters adopted special configurations that yielded also singular spectra.

When there were H-bonds, the characteristic vibration of the O…H-O structure was usually very strong and appeared at the lowest wavenumber range, below 3600 cm^{-1}, and in one case below 3100 cm^{-1}, for the strongest H-bonded system found among these samples.

The calculated spectra were compared to those observed by Kouchi *et al*.[22] at a deposition temperature of 10 K. Since the calculations were carried out in the harmonic approximation, an anharmonicity correction was applied with 1 % reduction in the calculated wavenumbers. This yielded a reasonable agreement with the observations, and in particular, confirmed the hypothesis advanced in Kouchi *et al*.[22] that linked the observed peaks at 3707 and 3617 cm^{-1} to the presence of unbound water molecules in their water-poor samples.

Finally, a test study on the residual pressure in the cells was carried out by means of calculations with fixed or variable size of the cell. The results were in agreement with the expectations, opening the path for further calculations to be attempted in the future.

Acknowledgments

This study was supported by a Grant for the Joint Research Program of the Institute of Low Temperature Science, Hokkaido University, Project i-link 1027 from CSIC, Project FIS2013-48087-C2-1-P from MINECO, Spain, JSPS KAKENHI (Grant Number 25247086), and MEXT KAKENHI (Grant Number 25108002). Calculations have been performed at westgrid, Canada, and CESGA and Trueno, CSIC, Spain. We are grateful for computing support from these Institutions. We also thank Dr. P. C. Gómez and Prof. V. J. Herrero for helpful comments on the manuscript.

References

1 W. Hagen and A.G.G.M. Tielens, *J. Chem. Phys.*, 1981, **75**, 4198.

2 A. Kouchi, *J. Crystal Growth.,* 1990, **99**, 1220.

3 A. Givan, A. Loewenschuss and C. J. Nielsen, *J. Chem. Soc. Faraday Trans.,* 1996, **92**, 4927.

4 G. M. Muñoz Caro, Y.-J. Chen, S. Aparicio, A. Jiménez-Escobar, A. Rosu-Finsen, J. Lasne and M. R. S. McCoustra, *Astron. & Astrophys*., 2016, **589,** A19.

5 T. Lauck, L. Karssemeijer, K. Shulenberger, M. Rajappan, K.I. Öberg and H. M. Cuppen, *Astrophys. J.*, 2015, **801**:118.

6 Y.-J. Chen, K.-J. Chuang, G. M. Muñoz Caro, M. Nuevo, C.-C. Chu2, T.-S. Yih2, W.-H. Ip, and C.-Y. R. Wu, *Astrophys. J.,* 2014, **781**:15.

7 F. Mispelaer, P. Theulé, H. Aouididi, J. Noble, F. Duvernay, G. Danger, P. Roubin, O. Morata, T. Hasegawa and T. Chiavassa, *Astron & Astrophys.*, 2013, **555**, A13.

8 M. Bertin, E.C. Fayolle, C. Romanzin, H.A. Poderoso, X. Michaut, L. Philippe, P. Jeseck, K.I. Öberg, H. Linnartz and J.-H. Fillion, *Astrophys. J.*, 2013, **119:**120.

9 E.C. Fayolle, M. Bertin, C. Romanzin, X. Michaut, K.I. Öberg, H. Linnartz and J.-H. Fillion, *Astrophys. J. Lett.,* 2011, **739:**L36.

10 K.I. Öberg, G. W. Fuchs, Z. Awad, H. J. Fraser, S. Schlemmer, E.F. van Dishoeck and H. Linnartz, *Astrophys. J.*, 2007, **662**, L23.

11 M. E. Palumbo, G. A. Baratta, M. P. Collings and M. R. S. McCoustra, *Phys. Chem. Chem. Phys.*, 2006, **8**, 279.

12 M. P. Collings, J. W. Dever, H. J. Fraser, M. R. S. McCoustra and D. A. Williams, *Astrophys. J.*, 2003, **583**, 1058.

13 A. Givan, A. Loewenschuss and C. J. Nielsen, *Vib. Spectrosc.*, 1998, **16**, 85.

14 S.A. Sandford, L.J. Allamandola, A.G.G.M. Tielens and G.J. Valero, *Astrophys. J.* ,1988, **329**, 498.

15 M. D Brookes and A. R. W. McKellar, *J. Chem. Phys*., 1998, 109, 5823.

16 A.I. Vasyunin and E. Herbst, *Astrophys. J.*, 2013, **769**:34.

17 S. Ioppolo, Y. van Boheemen, H.M. Cuppen, E.F. van Dishoeck and H. Linnartz, *Mon. Not. R. Astron. Soc.*, 2011, **413**, 2281.

18 D. C. Lis, G. A. Blake and E. Herbst, eds. of *Astrochemistry: Recent Successes and Current Challenges (IAU S231),* Cambridge University Press, 2006. Several chapters deal with this subject.

19 N. Watanabe and A. Kouchi, *Astrophys. J. Lett.,* 2002, **571**, L173.

20 L.J. Karssemeijer, S. Ioppolo, M.C. van Hemert, A. van der Avoird, M.A. Allodi, G.A. Blake and H.M. Cuppen, *Astrophys. J.*, 2014, **781**:16.

21 P.F. Fracassi, G. Cardini, S. O'Shea, R. W. Impery and M.L. Klein, *Phys. Rev. B,* 1986, **33**, 3441.

22 A. Kouchi, T. Hama, Y. Kimura, H. Hidaka, R. Escribano and N. Watanabe, *Chem. Phys. Lett.,* 2016, **658**, 287.

23 R.L. Mills, B. Onlinger and D.T. Cromer, *J. Chem. Phys.*, 1986, **84**, 2837.

24 L. von Vegard, *Z. Phys.*, 1930, **61**, 185.

25 S. J. Clark, M. D. Segall, C. J. Pickard, P. J. Hasnip, M. I. J. Probert, K. Refson and M. C. Payne, *Z. Kristalogr.*, 2005, **220**, 567.

26 Materials Studio v8, Accelrys-Biovia webpage http://accelrys.com/, Dassault Systèmes, 2014.

27 M.H. Lee, PhD Thesis, Cambridge University (1996).

28 J. P. Perdew, K. Burke and M. Ernzerhof, *Physical Review Letters*, 1996, **77**, 3865.

29 D. Sánchez-Portal, P. Ordejón, and E. Canadell, *Struct. Bond.,* 2004, **113**, 103.

30 J.M. Soler, E. Artacho, J.D. Gale, A. García, J. Junquera, P. Ordejón, and D. Sánchez-Portal, *J. Phys.: Cond. Matter*, 2002, **14**, 2745.

31 P. Ordejón, E. Artacho and J. M. Soler, *Phys. Rev. B*,1996, **53**, 10441.

32 E. Artacho, D. Sánchez-Portal, P. Ordejón, A. García and J. M. Soler, *Phys. Stat. Sol. (b),* 1999, **215**, 809.

33 N. Troullier and J.L. Martins, *Phys. Rev. B*, 1991, **43**, 1993.

34 B. Martín-Llorente, D. Fernández-Torre and R. Escribano, *Chem. Phys. Chem.*, 2009, **10**, 3229.

Supplementary Material

Table S1. Initial and final structures of the water molecules in all samples studied in this work. *mon* is used to represent unbound water molecules and W…W to indicate water molecules linked by a H-bond with O…H ≤ 2.2 Å. The O…H distance of the H-bond is quoted in Å.

	Initial	Final
	Structure (H-bond distance/Å)	Structure (H-bond distance/Å)
large-matrix (from 32 CO matrix)		
30CO-2W-a	mon,mon	mon,mon
30CO-2W-b	mon,mon	mon,mon
30CO-2W-c	W…W (1.9)	W…W (1.9)
29CO-3W-a	mon,W…W (2.0)	mon,W…W (2.2)
29CO-3W-b	W…W…W (1.9,1.9)	W…W…W (1.9,1.9)
28CO-4W	mon,mon,W…W (2.0)	mon,W…W…W (2.1,2.1)
small-matrix (from 16 CO matrix)		
14CO-2W-a	W…W (2.1)	W…W (1.9)
14CO-2W-b	mon,mon	W…W (1.9)
14CO-2W-c	mon,mon	mon,mon
14CO-2W-d	mon,mon	mon,mon
13CO-3W-a	mon,W…W (1.9)	mon,W…W (1.9)
13CO-3W-b	mon,W…W (2.0)	mon,W…W (1.9)
13CO-3W-c	mon,W…W (2.2)	mon,W…W (2.0)
13CO-3W-d	mon,W…W (2.2)	W…W…W (1.9,1.9)
12CO-4W-a	mon,mon,mon,mon	mon,W…W…W (1.8,1.9)
12CO-4W-b	mon,mon,mon,mon	mon,mon,mon,mon
12CO-4W-c	mon,mon,W…W (1.9)	mon,mon,W…W (1.9)
12CO-4W-d	W…W,W…W (2.0,2.0)	W…W…W…W (1.9,1.9,2.0)
H2O clusters		
29CO-triW-lin[a]	W…W…W (1.8,1.9)	W…W…W (1.8,1.8)
29CO-triW-ang[a]	W…W…W (1.9,1.9)	W…W…W (1.8,1.8,2.0[b])
28CO-tetraW-lin[a]	W…W…W…W (1.9,2.0,2.0)	W…W…W…W (1.8,1.8,1.9)
28CO-tetraW-ang[a]	W…W…W…W (1.8,1.8,1.8)	W…W…W…W (1.8,1.8,1.8)
25CO-triW-tetraW-lin	W…W…W;W…W…W…W (1.8,1.9;1.9,1.9,2.0)	W…W…W…W…W…W…W (1.7,1.8,1.8,1.8,1.8,2.0[b])
13CO-triW-lin[a]	W…W…W (1.8,1.9)	W…W…W (1.7,1.7)[c]
13CO-triW-ang[a]	W…W…W (1.9,1.9,1.9[b])	W…W…W (1.9,1.9,2.0[b])
12CO-tetraW-lin[a]	W…W…W…W (1.9,2.0,2.0)	W…W…W…W (1.8,1.8,1.9)
12CO-tetraW-ang[a]	W…W…W…W (1.8,1.8,1.8)	W…W…W…W (1.8,1.8,1.8)
11CO-pentaW-lin[a]	W…W…W;W…W (1.7,1.8;1.8)	W…W…W…W…W (1.8,1.8,1.8,1.9)
Amorphous		
13CO-triW-lin-amorp[a]	mon,mon,mon	mon,W…W (1.8)
13CO-triW-ang-amorp[a]	mon,mon,mon	W…W…W (1.9,2.0)

[a]Initial structure of clusters calculated for the isolated species

[b]Closed ring structure

triW-lin

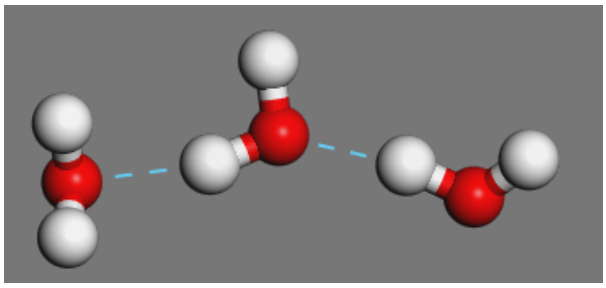

triW-ang

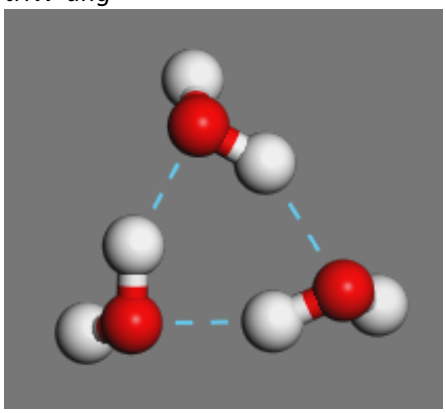

tetraW-lin

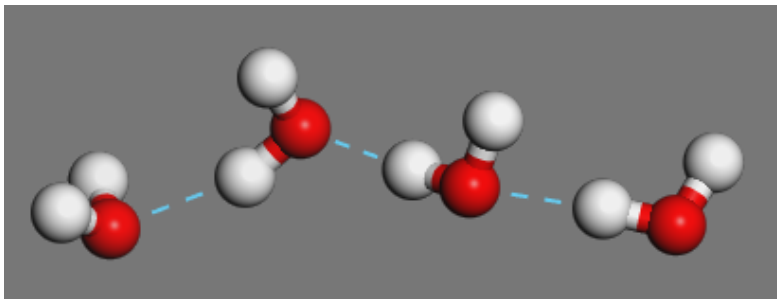

tetraW-ang

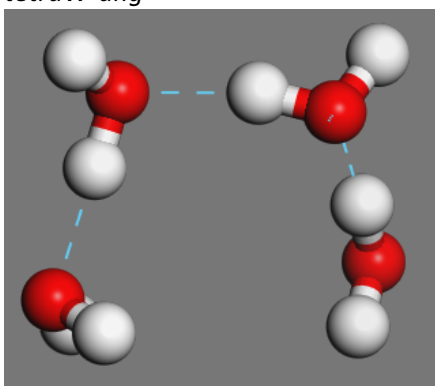

Fig. S1. Water clusters with 3 and 4 molecules. Optimized structures adopt quasi-linear and quasi-closed (angular) configurations.